# Scroll Wave Dynamics in a Three-Dimensional Cardiac Tissue Model: Roles of Restitution, Thickness, and Fiber Rotation

Zhilin Qu, Jong Kil, Fagen Xie, Alan Garfinkel, and James N. Weiss
Cardiovascular Research Laboratory, Departments of Medicine (Cardiology), Physiology, and Physiological Science, University of California, Los Angeles, California 90095 USA

ABSTRACT Scroll wave (vortex) breakup is hypothesized to underlie ventricular fibrillation, the leading cause of sudden cardiac death. We simulated scroll wave behaviors in a three-dimensional cardiac tissue model, using phase I of the Luo-Rudy (LR1) action potential model. The effects of action potential duration (APD) restitution, tissue thickness, filament twist, and fiber rotation were studied. We found that APD restitution is the major determinant of scroll wave behavior and that instabilities arising from APD restitution are the main determinants of scroll wave breakup in this cardiac model. We did not see a "thickness-induced instability" in the LR1 model, but a minimum thickness is required for scroll breakup in the presence of fiber rotation. The major effect of fiber rotation is to maintain twist in a scroll wave, promoting filament bending and thus scroll breakup. In addition, fiber rotation induces curvature in the scroll wave, which weakens conduction and further facilitates wave break.

## INTRODUCTION

Numerous experiments suggest that scroll waves (or their two-dimensional (2D) analogs, spiral waves) are a major cause of reentrant cardiac arrhythmias (Allessie et al., 1973; Chen et al., 1988; Davidenko et al., 1992; Winfree, 1994a; Gray et al., 1995, 1998; Chen et al., 1997; Witkowski et al., 1998). In particular, ventricular fibrillation, the leading cause of sudden cardiac death, has been identified with spiral or scroll wave breakup, in which wavelets are continually being created and destroyed (Janse and Wit, 1989; Lee et al., 1996; Garfinkel et al., 1997; Kim et al., 1997; Witkowski et al., 1998; Weiss et al., 1999; Garfinkel and Qu, 1999). If this is true, then understanding the determinants of scroll wave stability becomes extremely important. Studies of 2D homogeneous cardiac tissue models have shown that the transition from a single spiral wave to spiral wave breakup occurs when the slope of the action potential duration (APD) restitution relation becomes sufficiently steep (Karma, 1994; Courtemanche, 1996; Qu et al., 1999a). In three dimensions (3D), however, the situation is much less clear. Most 3D studies of scroll waves have been carried out in Fitzhugh-Nagumo (FHN)-type models (Keener and Tyson, 1992; Winfree, 1994b; Panfilov and Keener, 1995; Biktashev, 1998; Gray and Jalife, 1998; Berenfeld and Pertsov, 1999), which grossly oversimplify cardiac electrophysiology. Several of these studies showed that scroll wave breakup can occur in tissue that is sufficiently thick in the third dimension, while the corresponding 2D spiral wave remains intact. However, FHN-type models lack a key property of cardiac tissue: APD restitution, which has been shown to be very important for the stability of reentry (Karma, 1994; Courtemanche, 1996; Qu et al., 1999a).

In addition, real cardiac tissue contains significant preexisting heterogeneities, such as fiber rotation and endo- to epicardial and base-to-apex electrophysiological differences. Recently, Panfilov and Keener (1995) showed that fiber rotation could cause scroll wave breakup in the FHN type model. Fenton and Karma (1998a,b) simulated the effect of fiber rotation on the stability of scroll waves, using a simplified Beeler-Reuter action potential model. Their major conclusion was that fiber rotation created regions of highly localized filament twist, called "twistons." These twistons migrate toward the boundaries of the tissue; when a twiston collides with a boundary it causes a scroll wave filament to break, producing daughter scroll waves.

However, the connection between these results and actual wave instabilities in cardiac tissue is uncertain, because the stability of scroll waves is model-dependent, and the cell models used in these studies are highly simplified compared to real cardiac cells. Therefore, it is important to carry out simulations in physiologically more realistic models. In this paper, we used a 3D tissue model with phase I of the Luo-Rudy (LR1) action potential model (Luo and Rudy, 1991), which contains physiologically realistic formulations of most cardiac ionic currents. We studied how scroll wave stability is affected by electrical restitution, tissue thickness, initial filament twist, and fiber rotation. Our major conclusion is that steep APD restitution remains the primary cause of wave instability in 3D tissue, as it is in 2D, with tissue thickness, filament twist, and fiber rotation playing ancillary roles.

*Received for publication 23 November 1999 and in final form 1 March 2000.*

Address reprint requests to Dr. Zhilin Qu, Cardiovascular Research Laboratory, MRL 3645, UCLA School of Medicine, 675 Charles E. Young Dr. South, Los Angeles, CA 90095-1760. Tel.: 310-794-7027; Fax: 310-206-5777; E-mail: zqu@ucla.edu.



0006-3495/00/06/2761/15 $2.00

## METHODS

### Mathematical model

The partial differential equation (PDE) for cardiac conduction is (Panfilov and Holden, 1997)

$$\partial_t V = -I_{ion}/C_m + \nabla \cdot \tilde{D} \nabla V, \quad (1)$$

where $V$ is the transmembrane potential, $C_m$ is the membrane capacitance, and $I_{ion}$ is the total ionic current density of the membrane. $\tilde{D} = \tilde{\sigma}/S_v C_m$ is the diffusion tensor, where $\tilde{\sigma}$ is the conductivity tensor and $S_v$ is the surface-to-volume ratio of the cell. We used no flux boundary condition (Fenton and Karma, 1998b; Berenfeld and Pertsov, 1999): $\hat{n} \cdot (\tilde{D} \nabla V) = 0$, where $\hat{n}$ is the unit vector normal to the boundary. In a 3D system, $\tilde{D}$ has the following matrix structure (Panfilov and Holden, 1997; Vetter and McCulloch, 1998):

$$\tilde{D} = \begin{pmatrix} D_{xx} & D_{xy} & D_{xz} \\ D_{yx} & D_{yy} & D_{yz} \\ D_{zx} & D_{zy} & D_{zz} \end{pmatrix}. \quad (2)$$

We used the LR1 action potential model, in which the total ionic current is $I_{ion} = I_{Na} + I_{si} + I_K + I_{K1} + I_{Kp} + I_b$, where $I_{Na} = \bar{G}_{Na} m^3 hj(V - E_{Na})$ is the fast inward $Na^+$ current; $I_{si} = \bar{G}_{si} df(V - E_{si})$ is the slow inward current, assumed to be the L-type $Ca^{2+}$ current; $I_K = \bar{G}_K x x_1 (V - E_K)$ is the slow outward time-dependent $K^+$ current; $I_{K1} = \bar{G}_{K1} K1_\infty (V - E_{K1})$ is the time-independent $K^+$ current; $I_{Kp} = 0.0183 K_p (V - E_{Kp})$ is the plateau $K^+$ current; and $I_b = 0.03921(V + 59.87)$ is the total background current. $m$, $h$, $j$, $d$, $f$, and $x$ are gating variables satisfying the following type of differential equation:

$$dy/dt = (y_\infty - y)/\tau_y, \quad (3)$$

where $y$ represents the gating variables. $y_\infty$ and $\tau_y$ are functions of $V$. The ionic concentrations are $[Na]_i = 18$ mM, $[Na]_o = 140$ mM, $[K]_i = 145$ mM, and $[K]_o = 5.4$ mM, while the intracellular $Ca^{2+}$ concentration obeys

$$d[Ca]_i/dt = -10^{-4} I_{si} + 0.07(10^{-4} - [Ca]_i). \quad (4)$$

Details of the LR1 action potential model were presented in Luo and Rudy's paper (Luo and Rudy, 1991). By setting $[K]_o = 5.4$ mM, the maximum conductance of $I_K$ and $I_{K1}$ are $\bar{G}_K = 0.282$ mS/cm$^2$ and $\bar{G}_{K1} = 0.6047$ mS/cm$^2$. $\bar{G}_{Na} = 23$ mS/cm$^2$ and $\bar{G}_{si} = 0.09$ mS/cm$^2$ were fixed in the LR1 model. The original LR1 model has an APD of ~360 ms and a very steep APD restitution curve. We have varied some of these parameters to study the scroll wave dynamics. We fixed $\bar{G}_{Na} = 16$ mS/cm$^2$ as in the later version of the Luo and Rudy model (Luo and Rudy, 1994) and $\bar{G}_K = 0.423$ mS/cm$^2$, but we varied $\bar{G}_{si}$ and $\tau_d$ and $\tau_f$ of the $Ca^{2+}$ channel to investigate various types of vortex dynamics. Most of our simulations were carried out with a twofold speedup of $Ca^{2+}$ kinetics, i.e., $\tau_d \rightarrow 0.5\tau_d$ and $\tau_f \rightarrow 0.5\tau_f$. When $\bar{G}_{si}$ is around 0.05 mS/cm$^2$, the baseline APD is around 200 ms; we refer to this case as normal. We changed $\bar{G}_{si}$ to alter the 2D spiral wave dynamics, allowing us to investigate the effects of tissue thickness and fiber rotation for different regimes of 2D spiral wave behavior.

The rationale for selecting the LR1 model instead of later versions (Luo and Rudy, 1994; Jafri et al., 1998; Chudin et al., 1999) that formulate intracellular $Ca^{2+}$ dynamics was as follows: 1) LR1 model is computationally much cheaper; 2) the 2D behavior of the LR1 model is clearer than that of the later versions; 3) there is slow drift in ion concentrations in the later versions (Xu and Guevara, 1998), which introduces artifacts that are difficult to eliminate.

## Numerical simulation

We implemented the model in various structures: a 1D cable, 2D homogeneous tissue, 3D homogeneous tissue, 3D tissue with fiber rotation, and a hollow cylinder with fiber rotation. The numerical method used in most cardiac simulations is the forward Euler method (Courtemanche et al., 1993; Pollard et al., 1993; Courtemanche, 1996; Efimov et al., 1995; Muzikant and Henriquez, 1998), although advanced numerical methods have been developed (Quan et al., 1998; Vigmond and Leon, 1999; Qu and Garfinkel, 1999). We integrated Eqs. 1–4, using an operator splitting and adaptive time step methods (Qu and Garfinkel, 1999). We split Eq. 1 into an ordinary differential equation (ODE), which is the reaction term

$$\partial_t V = -I_{ion}/C_m, \quad (5)$$

and a partial differential equation, which is the diffusion term

$$\partial_t V = \nabla \cdot \tilde{D} \nabla V. \quad (6)$$

ODEs for the gating variables (Eq. 3) were integrated with the method of Rush and Larsen (1978). Equations 3 and 4 were integrated by a first-order explicit method. Adaptive time step methods were used in integrating Eqs. 3–5; the time step varied from 0.02 to 0.2 ms. The PDE (Eq. 6) was integrated by using a first-order explicit method with time step that was a fraction of 0.2 ms to satisfy the stability requirement. The space step was fixed at 0.015 cm in all simulations. Integration of ODEs and PDE was carried out alternatively as required by the operator splitting method. The spatial discretization of Eq. 6 is a three-point centered difference for 1D, a five-point centered difference for 2D, a seven-point centered difference for 3D homogeneous tissue, and the centered difference scheme in Fenton and Karma (1998b) for 3D with fiber rotation. The details on the numerical stability and accuracy of the splitting method in 2D simulation were presented previously by Qu and Garfinkel (1999). Here we directly adopted this method for the 3D case, using a time step of 0.025 ms to integrate Eq. 6.

### 1D cable

In Eq. 1, if all of the elements of the tensor $D$ are set to zero except $D_{xx}$, then Eq. 1 becomes a 1D cable equation. We set $D_{xx} = 0.001$ cm$^2$/ms.

### 2D homogeneous tissue

In Eq. 1, if all of the elements of $D$ are set to zero except $D_{xx}$ and $D_{yy}$, we obtain the cable equation for 2D homogeneous tissue. We set $D_{xx} = D_{yy} = 0.001$ cm$^2$/ms.

### 3D homogeneous tissue

In Eq. 1, if the elements of $D$ are set to zero, except for $D_{xx}$, $D_{yy}$, and $D_{zz}$, we obtain the equation for 3D homogeneous tissue. We set $D_{xx} = D_{yy} = 0.001$ cm$^2$/ms, and $D_{zz} = 0.0002$ cm$^2$/ms.

### 3D tissue with fiber rotation

We assume that the fibers are parallel and uniform in the $x$–$y$ plane but rotate along the $z$ direction. Therefore, $\tilde{D}$ has the following matrix structure (Panfilov and Keener, 1995; Fenton and Karma, 1998b):

$$\tilde{D} = \begin{pmatrix} D_{xx} & D_{xy} & 0 \\ D_{yx} & D_{yy} & 0 \\ 0 & 0 & D_{zz} \end{pmatrix},$$

where

$$\begin{aligned} D_{xx} &= D_\parallel \cos^2\theta(z) + D_\perp \sin^2\theta(z) \\ D_{yy} &= D_\parallel \sin^2\theta(z) + D_\perp \cos^2\theta(z) \\ D_{xy} &= D_{yx} = (D_\parallel - D_\perp)\cos\,\theta(z)\sin\,\theta(z) \\ D_{zz} &= D_\perp . \end{aligned} \quad (7)$$

$D_{\parallel}$ is the diffusion constant along the fiber direction, and $D_{\perp}$ is the transverse diffusion constant. $\theta(z)$ is the twist angle along the $z$ direction. We used a uniform fiber rotation angle $\theta(z) = \alpha z$. The total angle of fiber rotation from endocardium to epicardium is $\theta = \alpha L_z$. In this paper, we used $D_{\parallel} = 0.001$ cm$^2$/ms and $D_{\perp} = 0.0002$ cm$^2$/ms (Fenton and Karma, 1998b).

### *Hollow cylinder with fiber rotation*

We also simulated reentry on the surface of a hollow cylinder with fiber rotation. In this case, the diffusion term in Eq. 6 becomes

$$\nabla \cdot \tilde{D}\nabla = [(D_{xx} - D_{yy})\sin 2\varphi - 2D_{xy}\cos 2\varphi]\frac{\partial}{R^2\partial\varphi} + (D_{xx}\sin^2\varphi + D_{yy}\cos^2\varphi - D_{xy}\sin 2\varphi)\frac{\partial^2}{R^2\partial\varphi^2} + D_{zz}\frac{\partial^2}{\partial z^2}, \quad (8)$$

where $R$ is the radius of the cylinder. $D_{xx}$, $D_{xy}$, $D_{yy}$, and $D_{zz}$ are taken from Eq. 7. A five-point centered difference scheme was used. To keep the same spatial resolution, $\Delta\varphi = 0.015$ cm/$R$ was used in integrating Eq. 8.

### *Measuring APD restitution*

We defined APD by the duration during which $V > -72$ mV, while DI was defined by the duration during which $V < -72$ mV. APD restitution was calculated in a 1D cable paced at one end. By slowly and progressively increasing the pacing rate, we obtained APD restitution curves.

### *Measuring spiral tip, vortex filament, and tip velocity*

The location of the spiral tip in 2D was calculated by the intersection of two successive isovoltage lines at a time interval of 1 or 2 ms, using $-30$ mV as the threshold for the isovoltage lines. These tips, one for each $z$ level, formed the filament of the 3D scroll wave. We also used the tip positions to calculate tip velocity and twist angle, which we defined as the difference between the direction of tip movement at a layer and the direction of tip movement in the endocardium (see Fig. 8).

## RESULTS

As mentioned above, we and others have previously argued that spiral wave dynamics in 2D tissue are governed largely by electrical restitution properties (Karma, 1994; Courtemanche, 1996; Qu et al., 1999a). By altering $Ca^{2+}$ current amplitude and kinetics (Qu et al., manuscript submitted for publication) in the LR1 model in 2D tissue, distinct spiral wave phenotypes can be generated, including stable, weak meander, strong meander, and breakup. The strategy in this study was to determine how the third dimension affects the corresponding scroll wave behavior when these spiral wave phenotypes are placed in 3D tissue. Specifically, we studied the roles of restitution, tissue thickness, initial filament twist, and fiber rotation, respectively.

### Spiral wave behaviors in homogeneous 2D tissue

APD restitution refers to the curve relating APD to the previous diastolic interval (DI). From detailed investigation of spiral wave meander and breakup in the LR1 model (Qu et al., manuscript submitted for publication), we found that in 2D, chaotic meander and spiral wave breakup are caused by a APD restitution slope greater than 1. When APD restitution slope is smaller than 1 everywhere, only stable (period 1) spiral waves or quasiperiodically meandering spiral waves exist. Fig. 1 *A* shows the APD restitution curve for the LR1 model with normal $Ca^{2+}$ current kinetics, and Fig. 1 *B* shows the curve for the LR1 model with $Ca^{2+}$ current kinetics sped up by a factor of 2. In both cases, the slope of APD restitution increased as $\bar{G}_{si}$ increased, but in Fig. 1 *A*, the steepening occurred uniformly, whereas in Fig. 1 *B*, the steepening was restricted to short DI's, with the APD restitution slope reduced at long DI's. (Thus, in the latter case, maximum APD restitution slope was increased, but the range of DI's with a slope greater than 1 was reduced.) Fig. 1, *C* and *D*, shows the corresponding spiral wave behaviors for the two cases. With normal $Ca^{2+}$ current kinetics (Fig. 1 *C*), the spiral wave was stable at low $\bar{G}_{si}$ and developed progressively more violent meander as $\bar{G}_{si}$ increased, leading to spontaneous breakup near $\bar{G}_{si} = 0.045$ mS/cm$^2$. With the $Ca^{2+}$ current kinetics sped up (Fig. 1 *D*), the meandering behavior was extended over a wider range of $\bar{G}_{si}$ and was more violent before breakup, which occurred at $>0.065$ mS/cm$^2$ (similar to the findings of Courtemanche, 1996, who used the Beeler–Reuter model). Although addressed elsewhere (Qu et al., manuscript submitted for publication), CV restitution, in addition to APD restitution, also alters spiral wave behavior.

In this paper, we refer to the period 1 spiral wave in Fig. 1, *Ca* and *Da*, as *stable*; the meander shown in Fig. 1, *Cb–d* and Fig. 1 *D*, *b* and *c*, as *weak meander*; the meander shown in Fig. 1 *Dd–g* as *strong meander*; and spontaneous breakup into multiple spirals, shown in Fig. 1 *Ce*, as *breakup*. Weak and strong meander can be either quasiperiodic or chaotic. Note that the transition from weak meander to strong meander and breakup corresponds to increased steepness of APD restitution.

### Scroll wave dynamics in homogeneous 3D tissue—do tissue thickness and initial filament twist cause spiral wave breakup?

Having identified appropriate parameters to control 2D spiral wave phenotype, we next studied the corresponding scroll wave phenotypes in homogeneous 3D tissue. First we examined the stability of a straight scroll filament against small perturbations, to address the issue of whether tissue thickness can by itself induce scroll filament instability in the LR1 model, as has been seen in some simplified models

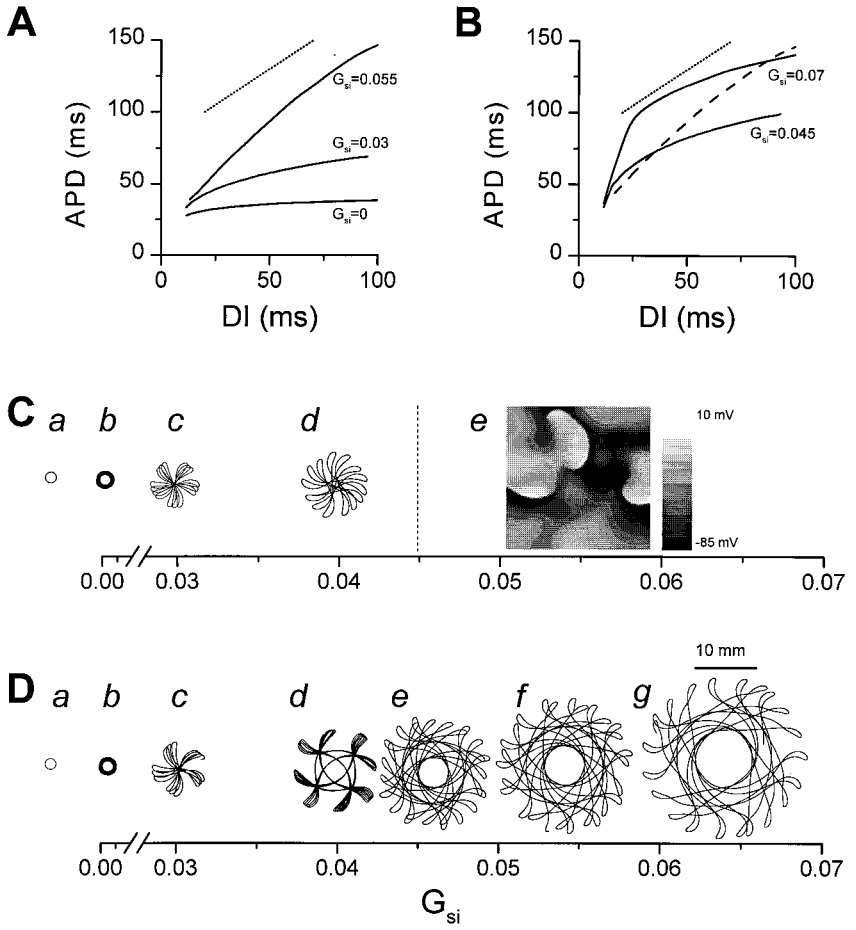


FIGURE 1 APD restitution curves and 2D spiral wave phenotype as a function of maximum $Ca^{2+}$ current conductance $\bar{G}_{si}$ in the LR1 model, with either normal $Ca^{2+}$ current kinetics (*A* and *C*), or with kinetics sped up by a factor of 2 (*B* and *D*). (*A*) APD restitution curves for $\bar{G}_{si} = 0$, 0.03, and 0.055 mS/cm$^2$ with normal $Ca^{2+}$ current kinetics. (*B*) APD restitution curves for $\bar{G}_{si} = 0.045$ and 0.07 mS/cm$^2$ with $Ca^{2+}$ kinetics sped up, i.e., $\tau_d \rightarrow 0.5\tau_d$ and $\tau_f \rightarrow 0.5\tau_f$. The dashed line in *B* is a redrawing of the APD restitution curve for $\bar{G}_{si} = 0.055$ mS/cm$^2$ in *A*. The dotted lines in *A* and *B* are reference lines of slope 1. (*C*) Spiral wave behaviors with normal $Ca^{2+}$ current kinetics. *a*: stable spiral ($\bar{G}_{si} = 0$, *j* gate clamped to 1); *b–c*: weak meander ($\bar{G}_{si} = 0$ and 0.03 mS/cm$^2$); *d*: strong meander ($\bar{G}_{si} = 0.04$ mS/cm$^2$); *e*: breakup ($\bar{G}_{si} = 0.055$ mS/cm$^2$). (*D*) Spiral wave behaviors with $Ca^{2+}$ current kinetics sped up. *a*: stable spiral ($\bar{G}_{si} = 0$, *j* gate clamped to 1); *b–c*: weak meander ($\bar{G}_{si} = 0$ and 0.03 mS/cm$^2$); *d–g*: strong meander ($\bar{G}_{si} = 0.04$, 0.045, 0.05, or 0.06 mS/cm$^2$). The spiral tip trajectories were all plotted on the same spatial scale (shown in *Dg*). In *Ce*, the tissue size is 4.8 cm × 4.8 cm. The same gray scale as shown in *Ce* was used for all snapshots in subsequent figures.

(Aranson and Bishop, 1997; Gray and Jalife, 1998; Biktashev, 1998; Nam et al., 1998; Qu et al., 1999b).

### *The role of tissue thickness*

To study the stability of an initially straight scroll filament against small perturbations, we lined up identical spiral waves, stacked along the *z* direction to form a vertically straight scroll wave, and then gave a random perturbation to this state, i.e., $V(x, y, z, 0) = V_0(x, y, z, 0) + 10$ mV* (*random* − 0.5), in which $V_0(x, y, z, 0)$ is the 2D spiral wave solution and *random* is a random number uniformly distributed in [0, 1]. We define a quantity,

$$s(t) = \frac{1}{L_x L_y L_z} \iiint_{xyz} [V(x, y, z, t) - \bar{V}(x, y, z, t)]^2 dx\, dy\, dz, \tag{9}$$

to measure the growth rate of this perturbation, where $\bar{V}(x, y, z, t) = (1/L_z) \int_z V(x, y, z, t) dz$, and $L_x$, $L_y$, and $L_z$ are the dimensions of the tissue. Note that $s(t)$ is the integral over all space of the distance between the actual value of $V$ at a point $(x, y, z)$ and the value of $V$ at that $(x, y)$ point averaged over the $z$ axis. Thus, if $s(t)$ decays to zero, then the straight vortex filament is stable; otherwise it is unstable.

*Stable, weak meander, and strong meander regimes.* Fig. 2 compares $s(t)$ for scroll waves corresponding to stable, weak meander, and strong meander regimes of 2D spiral waves (Fig. 1 *D*, *a*, *c*, and *e*, respectively) in 9-mm-thick tissue. The initial perturbations became progressively damped over time, demonstrating that for these parameter ranges, scroll waves were stable against small perturbations. We also performed simulations in 15-mm-thick tissue, as well as other parameter regions in Fig. 1 *D*, and obtained similar results. In addition, using the LR1 model with the original $Ca^{2+}$ current kinetics, the comparable parameter regions shown in Fig. 1 *Ca–d* gave similar results.

Several previous studies (Aranson and Bishop, 1997; Gray and Jalife, 1998; Biktashev, 1998; Nam et al., 1998; Qu et al., 1999b) in excitable media with two-variable cell models have found that an instability can occur when the tissue thickness exceeds a certain critical value. In this instability, a small perturbation applied to a straight scroll wave leads to a helical scroll wave or to scroll wave breakup. We recently demonstrated that such instabilities are diffusion induced (Qu et al., 1999b) and model depen-

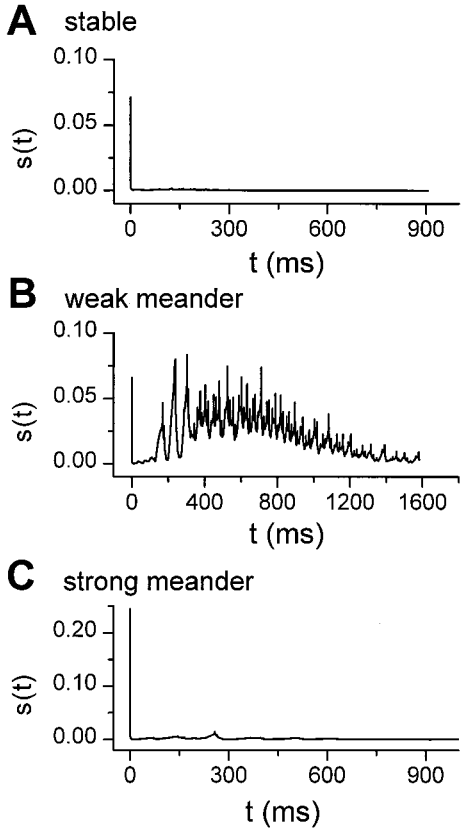


FIGURE 2 Stability of scroll filaments in homogeneous 3D tissue to small perturbations. $s(t)$ versus time for the scroll waves in the 2D stable (*A*), weak meander (*B*), and strong meander (*C*) regimes shown in Fig. 1 *D*. (*A*) $\bar{G}_{si} = 0, j = 1$; (*B*) $\bar{G}_{si} = 0.035$ mS/cm$^2$; (*C*) $\bar{G}_{si} = 0.045$ mS/cm$^2$. The tissue size was 3 cm × 3 cm × 0.9 cm in *A* and *B*, 4.8 cm × 4.8 cm × 0.9 cm in *C*.

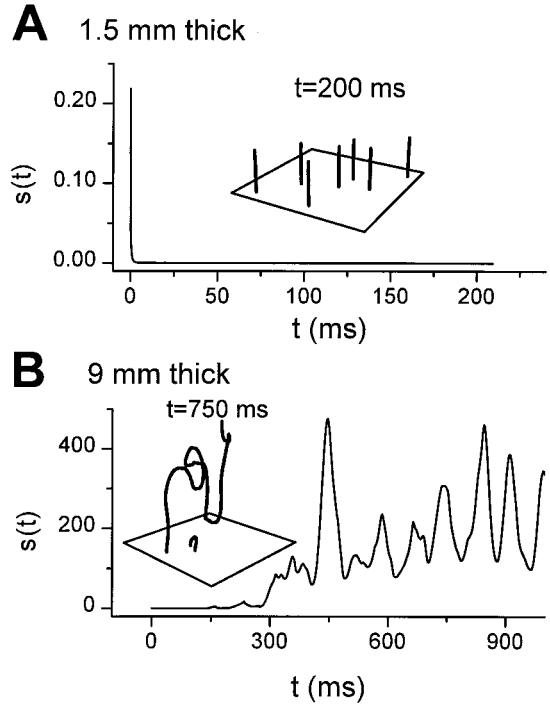


FIGURE 3 Effect of tissue thickness on filament stability in the breakup regime. $s(t)$ versus time for scroll breakup in 2D spiral wave breakup regime, comparing 0.15-cm-thick tissue (*A*) and 0.9-cm-thick tissue (*B*). The insets show the scroll filaments at 200 ms (*A*) and 750 ms (*B*). Parameters are the same as in Fig. 1 *Ce*.

dent. In the present model, we did not observe these instabilities. In summary, straight filaments were all stable in these parameter regimes, and no scroll breakup was found. Thus our findings indicate that a conversion from 2D no-breakup behavior to 3D breakup behavior, caused by tissue thickness, does not occur with the LR1 action potential model.

*Breakup regime.* To examine how breakup is affected by the presence of the third dimension, we implemented the LR1 model in the 2D breakup regime shown in Fig. 1 *Ce* and characterized the effects of tissue thickness on the filament stability. When the tissue was thinner than a critical value (~3 mm), the filaments were stable against small random perturbations, i.e., $s(t)$ finally decayed to zero (Fig. 3 *A*), even though the number of scrolls and their movements were chaotic. Thus chaotic motion in 2D was synchronized in the third dimension in thin tissue. When the tissue was thicker than the critical value, filament break occurred, resulting in transmural reentry. The system then displayed "fully developed turbulence" in 3D (Fig. 3 *B*). When the tissue thickness was only slightly greater than the critical value, filaments became unstable, and filament bending and twisting occurred. These findings demonstrate that the chaotic motions of the 2D spiral wave can be synchronized in the $z$ axis when the tissue is thin, but synchronization is lost when the thickness exceeds a critical length. (For discussions of spatiotemporal chaos synchronization and its relation to system size, see Heagy et al. (1995), Hu et al. (1995), Ding and Yang (1997), Yang et al. (1998), and Qu et al. (1999b).

### *The role of initial filament twist*

In the simulations described above, identical 2D spiral waves were stacked to form a straight vortex filament. To determine whether initial filament twist induces scroll breakup, we stacked up spiral waves from a 2D simulation at different phases, forming a twisted scroll vortex. Then we put this twisted scroll wave into 3D homogeneous tissue to study its behavior.

*Stable and weak meander regimes.* When parameters were such that the 2D spiral wave was in the stable or weak meander regimes, an initially twisted scroll wave became untwisted, finally forming a scroll wave with a straight filament, as shown in Fig. 4. The initial twist angles were over 300° from the top to bottom (i.e., "epicardial" to "endocardial") surfaces in a 9-mm-thick tissue. This corre-

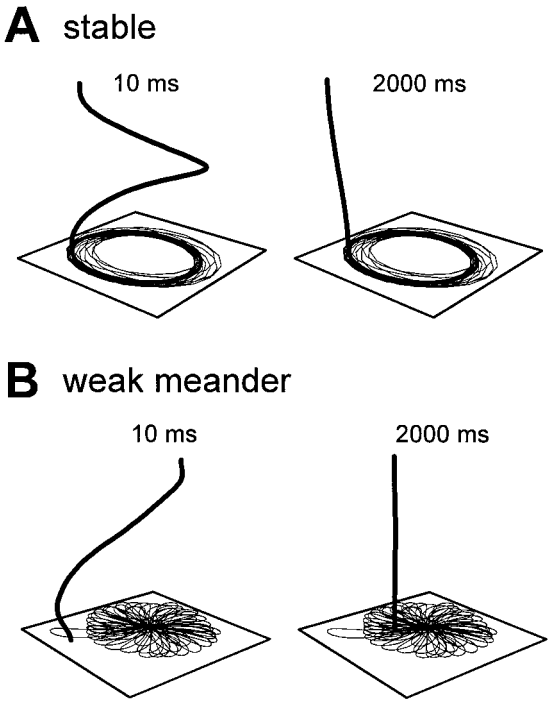


FIGURE 4 Straightening of initially twisted filaments in homogeneous 3D tissue, for the 2D stable (*A*) and weak meander (*B*) regimes (corresponding to Fig. 1 *D*, *a* and *e*). The scroll filaments at 10 and 2000 ms are shown as indicated, along with the continuously traced scroll tip trajectories on the bottom "endocardial" surface. (*A*) $\bar{G}_{si} = 0, j = 1$. (*B*) $\bar{G}_{si} = 0.035$ mS/cm$^2$. The time lags in initial conditions from the top to the bottom surfaces were 36 ms in *A* and 48 ms in *B*. Tissue size was 3 cm × 3 cm × 0.9 cm.

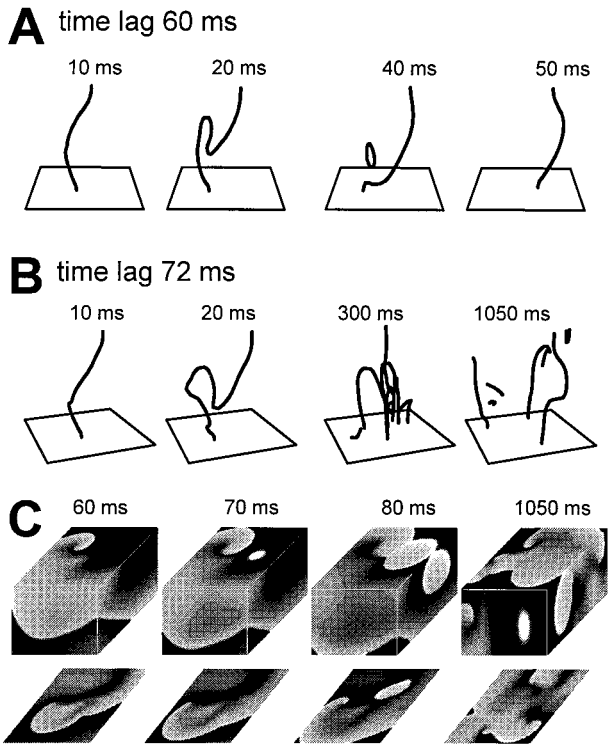


FIGURE 5 Filament break induced by initial filament twist in the 2D strong meander regime (corresponding to Fig. 1 *D*, $\bar{G}_{si} = 0.045$ mS/cm$^2$). (*A*) Time lag between the top and bottom surfaces (set in the initial conditions) of 60 ms. A scroll ring forms and then disappears. (*B*) Time lag, 72 ms. Complex filament breakup occurs. (*C*) Snapshots of scroll waves in *B*, showing the waves on the top "epicardial" surface, as well as on the forward-facing vertical surfaces. Below them are same waves on the bottom "endocardial" surface. The tissue size was 4.8 cm × 4.8 cm × 0.9 cm. The timing of each panel is indicated.

sponded to a time lag between the top and bottom surfaces of 36 ms for the stable spiral wave regime and 48 ms for the weak meander regime, i.e., about one rotation period. In both cases, the twisted filament became straight with time. Even with an initial twist angle of 720° (about two rotations) in the stable spiral wave regime, the scroll wave finally untwisted. Consistent with previous studies of twisted scroll waves in excitable media (Biktashev et al., 1994), we found that a twisted scroll wave rotated faster than an untwisted one.

*Strong meander regime.* In contrast to the stable and weak meander 2D regimes, a twisted scroll wave in the strong meander regime broke up if it was sufficiently twisted (Fig. 5). When the time lag from the top to the bottom surface was small, the scroll wave remained intact. No filament bending or break occurred, and the twisted filament eventually untwisted, becoming straight. At a critical time lag, however, filament bending occurred, leading to filament break. The break formed a new, less twisted filament plus a scroll ring (Fig. 5 *A*). The scroll ring finally shrank and disappeared, and the new filament eventually became untwisted. When the top-to-bottom time lag was even larger, filament bending led to very complex scroll breakup patterns (Fig. 5, *B* and *C*). We are not sure whether scroll breakup in this case was a sustained motion or a transient process, because of the limited computer run time.

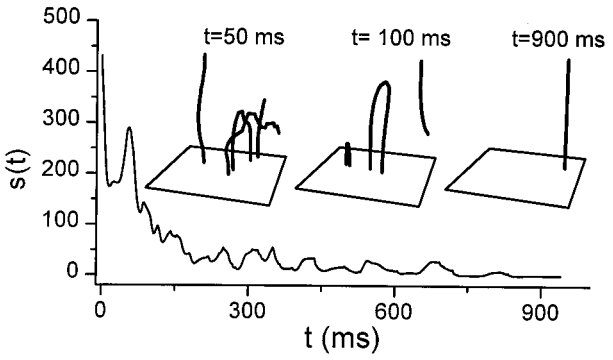


FIGURE 6 Scroll breakup due to an initially twisted filament in the 2D strong meander regime is transient. $s(t)$ versus time for the case shown in for Fig. 5 *B*, except that the tissue thickness has been reduced to 0.45 cm. Insets show filaments at 50, 100, and 900 ms.

However, in thinner tissue, breakup was transient, and finally only straight filaments were left in the tissue (Fig. 6).

We also simulated scroll waves close to the parameter boundary at which spiral wave breakup begins (Fig. 7). In this case, breakup did not occur if the time lag from top to bottom was small but did occur if the time lag was increased beyond a critical value. However, this breakup was not induced by filament bending. Instead, a scroll ring formed as a result of conduction block in the scroll wave arm, which was unrelated to filament collision. When the twist was large, the scroll ring expanded and collided with the tissue boundary, producing complex scroll breakup.

## Scroll wave behavior in inhomogeneous 3D tissue—does fiber rotation induce scroll wave breakup?

In real cardiac tissue, conduction is anisotropic, being faster parallel to fiber direction and slower transversely. Fiber direction also rotates from epicardium to endocardium through the ventricular wall, producing rotational anisotropy. To study 3D tissue with fiber rotation, we adjusted the diffusion coefficient to slow conduction velocity in one axis (transverse axis) while maintaining normal conduction velocity in the other (parallel axis). By convention, the parallel axis defines the fiber direction. Fiber direction was then rotated at a uniform rate along the $z$ axis between the top ("epicardial") and bottom ("endocardial") surfaces. We began with a scroll wave with a straight filament, composed of stacked-up identical spiral waves from 2D homogeneous tissue.

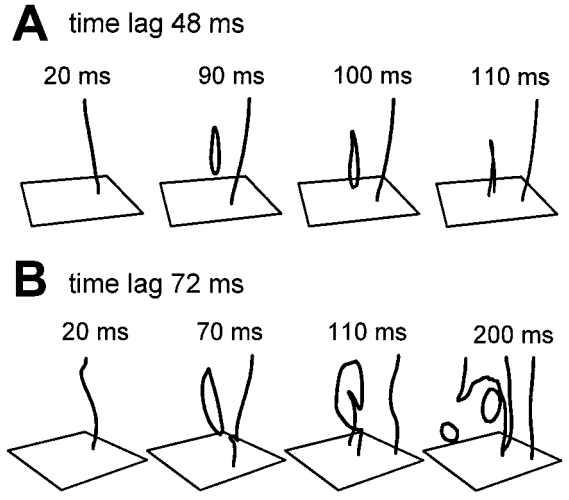


FIGURE 7 Scroll ring formation in the absence of filament collision, for the 2D strong meander regime. The strong meander regime was set very near the boundary for 2D breakup, with $\bar{G}_{si} = 0.048$ mS/cm$^2$, and $\tau_d \rightarrow 0.6\tau_d$, $\tau_f \rightarrow 0.6\tau_f$. (*A*) Time lag between the top and bottom surfaces (set in the initial conditions) of 48 ms. A small scroll ring forms independently without filament bending/collision and subsequently disappears. (*B*) Time lag, 72 ms. A larger scroll ring appears, leading to complex filament breakup. Tissue size was 4.8 cm × 4.8 cm × 0.9 cm.

### *Stable and weak meander regimes*

Fig. 8, *A* and *B*, shows the tip trajectories on the "epicardial" and "endocardial" surfaces for a stable 2D spiral wave (corresponding to Fig. 1 *Da*) as the tissue thickness (*A*) and degree of fiber rotation (*B*) were progressively increased. The scroll wave remained stable for any thickness and rotation rate up to 48°/mm. At 48°/mm, however, the filament began to drift. The drift still existed when we reduced $\Delta z$ to 0.0075 cm. We are uncertain whether this instability was real or was due to numerical inaccuracy.

Fig. 8 *C* shows a space-time plot of the filament twist angle from "endocardium" to "epicardium" in a 9-mm-thick tissue. The twist angle was measured as the angle between the direction in which the tip was moving in a given layer and the direction in which the tip moved on the endocardial surface, as illustrated in the insets between Fig. 8 *C* and Fig. 8 *D*. The maximum twist occurred between 3 and 6 mm along the $z$ axis, reaching nearly 80°, which was greater than the fiber rotation angle between 3 and 6 mm. In one period, the maximum twist angle occurred twice and the filament untwisted twice. Fig. 8 *D* shows the distance, projected in the $x$–$y$ plane, between the tip at various depths in the tissue and the tip on the "endocardial" surface. The maximum also occurred between 3 and 6 mm. Interestingly, the period of the scroll wave did not change with the fiber rotation rate, except for extremely large (>48°/mm) fiber rotation rates, at which the scroll wave rotated a little bit more slowly. In this regime, the cycle length for this scroll was always 35 ms. This differs from the rotation period of a twisted scroll wave in homogeneous tissue, which runs faster than a straight one (Biktashev et al., 1994).

Similar to the stable regime, in the 2D weak meander regime (corresponding to Fig. 1 *C*, *c* and *d*, and 1 *Dc*), a single scroll wave always remained intact. No breakup was observed, even at a fiber rotation rate up to 30°/mm in 9-mm-thick tissue. To further substantiate the robustness of these findings, we also changed APD restitution by speeding up the $Ca^{2+}$ kinetics (Xu and Guevara, 1998) by a factor of 10, i.e., $\tau_d \rightarrow 0.1\tau_d$ and $\tau_f \rightarrow 0.1\tau_f$. With this speedup, the slope of APD restitution was largely reduced and produced a 2D spiral wave with weak meander for $\bar{G}_{si} = 0.06$ mS/cm$^2$. We did not see scroll breakup with a fiber rotation rate of 18°/mm in 9-mm-thick 3D tissue (in the physiological range).

### *Strong meander regime*

In contrast to the stable or weak meander regimes, in the 2D strong meander regime, the resulting scroll wave behavior changed. For small degrees of fiber rotation, a scroll wave remained intact, with no filament bending or breakup. How-

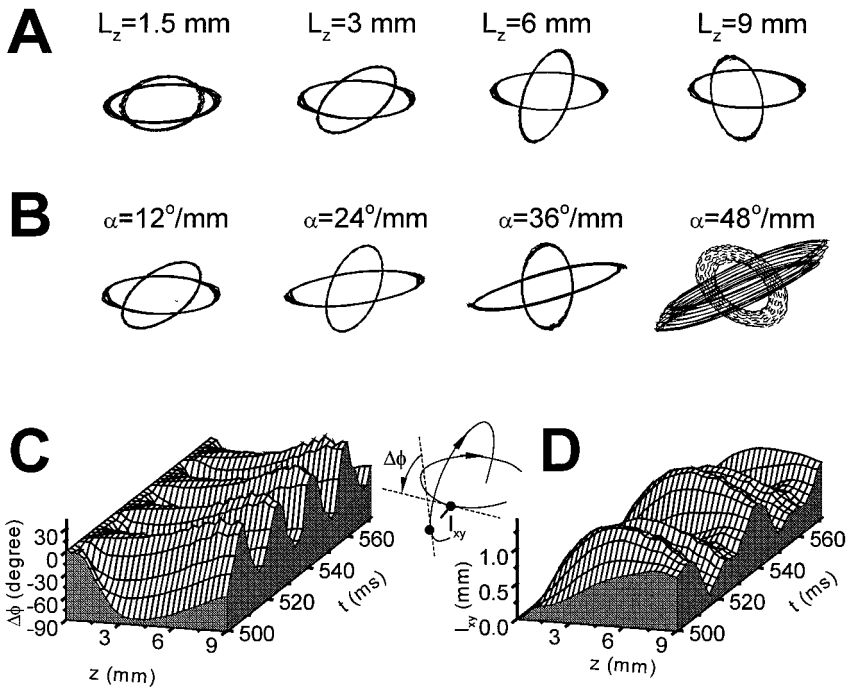


FIGURE 8 Effect of fiber rotation rate on filament bending in 3D tissue, for the 2D stable spiral regime (corresponding to Fig. 1 *Da*). Tip trajectories from the bottom "endocardial" surface (*dashed lines*) and the top "epicardial" surface (*solid lines*) are superimposed, for different tissue thickness ($L_z$) and fiber rotation rate ($\alpha$). (*A*) $\alpha$ = 12°/mm, $L_z$ = 1.5, 3, 6, and 9 mm, respectively. (*B*) $L_z$ = 3 mm, $\alpha$ = 12, 24, 36, and 48°/mm. (*C*) A plot of the angular difference ($\Delta\theta$) of propagation directions of the spiral tips in a given layer (depth $z$) relative to the endocardium (illustrated in the *inset*). The maximum differences occur at 3–6 mm depth. (*D*) A plot of the distance between the scroll tip in a given layer (depth $z$) and the scroll tip on the endocardium, projected in the $x$–$y$ plane, versus $t$ and $z$.

ever, when the fiber rotation rate was large, the scroll wave broke up. Fig. 9 shows the scroll filament in a 9-mm-thick tissue at a fiber rotation rate of 18°/mm. In the progression from the initially straight filament to scroll breakup, several distinct processes occurred:

First, filament bending occurred ($t$ = 50 ms). The bending filament collided with itself to form a small scroll ring ($t$ = 54 ms). This scroll ring shrank and disappeared; the bent filament straightened ($t$ = 70 ms).

Later, another scroll ring formed from the bent filament without collision ($t$ = 400–430 ms). This scroll ring expanded and broke at the boundaries ($t$ = 430 ms), while the bent filament straightened without forming new scroll rings or colliding with the boundary ($t$ = 430 ms).

Still later, a large scroll ring formed as the filament bent and collided with itself ($t$ = 570–600 ms); this scroll ring collided with one of the boundaries, producing breakup.

These processes occurred repeatedly and finally led to a pattern of complex scroll breakup in the tissue ($t$ = 800 and 850 ms).

Fig. 10 shows snapshots of the scroll waves corresponding to Fig. 9. Note that the spiral waves on the "endocardial" and "epicardial" surfaces became more and more desynchronized with time. Fenton and Karma (1998a,b) showed that filament unbending or the first filament break occurred when the bending filament collided with a boundary. We did not see this in our simulation in Fig. 9, but we did see this occur when the tissue was thinner. The filament behaviors in Fig. 9 for the tissue with fiber rotation were similar to the filament behaviors in Figs. 5 and 7 for twisted scroll waves in homogeneous tissue, except that breakup in the tissue with fiber rotation was sustained, while in homogeneous tissue it may have been transient because the scroll waves may finally have all untwisted.

After scroll breakup occurred, the average APD, average DI, and the average CL were shorter than in the case with no breakup. Fig. 11 shows the distribution of DI, APD, and CL for 2D strong meander (Fig. 1 *De*) and 3D scroll breakup (Fig. 9). The values for 3D were obtained after scroll wave breakup in the fully developed turbulent regime. Note that the curves from the 3D case were all shifted to the left with respect to the values in 2D in which the single spiral wave remained intact, with average values in 3D versus 2D: 19 versus 35 ms for DI; 52 versus 69 ms for APD; and 71 versus 104 ms for CL. Thus the average DI, APD, and CL in 3D were shorter by 45%, 25%, and 30%, respectively, because of scroll breakup.

When we explored the parameter space more fully, we found that whether a scroll wave broke up or not depended on three factors: $\bar{G}_{si}$, or equivalently, the APD restitution properties (which determine the 2D spiral wave dynamics), the fiber rotation rate, and tissue thickness, as summarized in Fig. 12. Fig. 12 *A* shows the relationship between the critical fiber rotation rate $\alpha_c$ at which scroll breakup occurred and $\bar{G}_{si}$ in a 9-mm-thick tissue. For $\bar{G}_{si} < 0.04$ mS/cm$^2$, scroll breakup did not occur, even at very large fiber rotation rates. At $\bar{G}_{si} = 0.04$ mS/cm$^2$, breakup was not observed until $\alpha$ exceeded 25°/mm. For $\bar{G}_{si} > 0.04$ mS/cm$^2$, $\alpha_c$ progressively decreased as $\bar{G}_{si}$ increased and was close to zero at $\bar{G}_{si} = 0.06$ mS/cm$^2$, at which 2D spiral waves are close to their breakup regime.

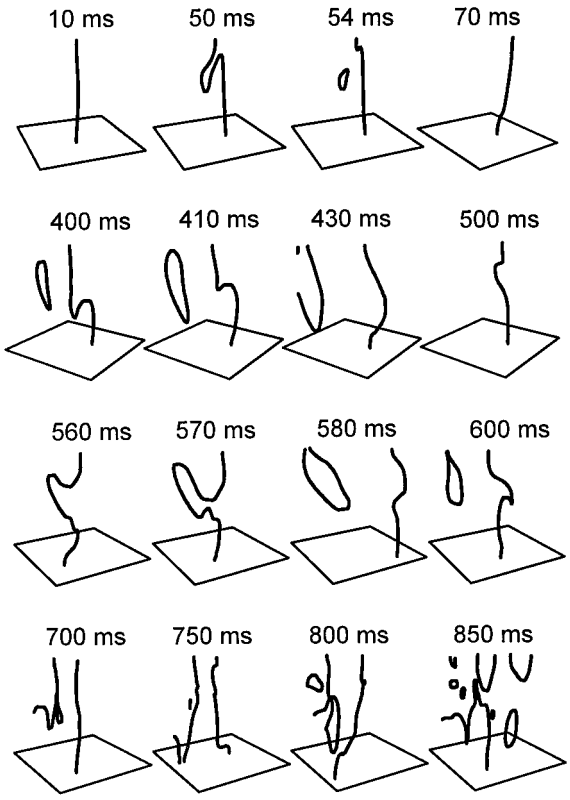


FIGURE 9 Filament breakup in 3D tissue with fiber rotation, for the 2D strong meander regime (corresponding to Fig. 1 *De*). Fiber rotation rate $\alpha = 18°/\text{mm}$. Tissue size: 4.8 cm × 4.8 cm × 0.9 cm. The time after initiation of the scroll wave is indicated above each panel.

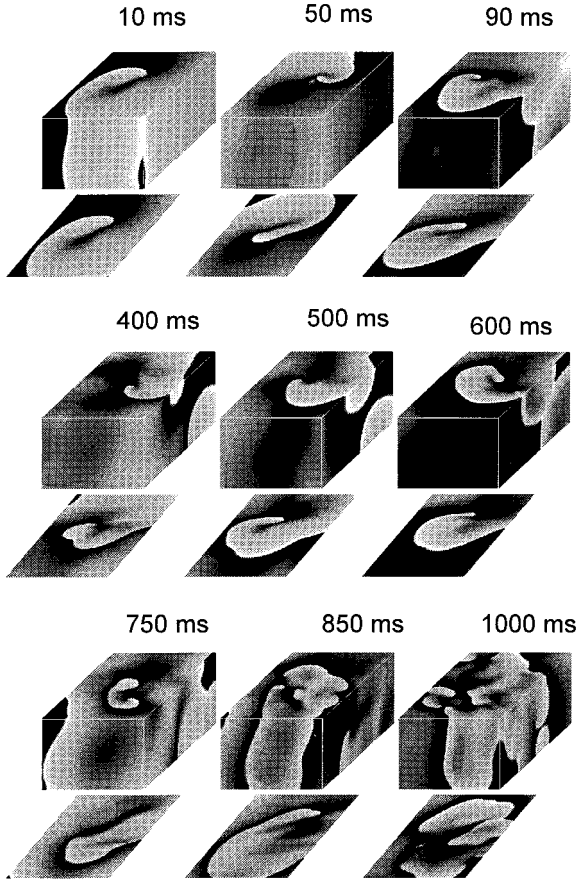


FIGURE 10 Snapshots for the simulation shown in Fig. 9, illustrating scroll breakup in 3D tissue with fiber rotation, for the 2D strong meander regime. Panels show the waves on the top "epicardial" surface, as well as on the forward-facing vertical surfaces. Below them are the same waves on the bottom "endocardial" surface.

Fig. 12 *B* shows the relationship between critical tissue thickness $L_c$ at which scroll breakup occurs and $\bar{G}_{si}$, for a fixed fiber rotation rate $\alpha = 15°/\text{mm}$. For $\bar{G}_{si} \leq 0.04$ mS/cm$^2$, scroll breakup did not occur in tissue up to 15 mm thick. For $\bar{G}_{si}$ between 0.045 and 0.06 mS/cm$^2$, the $L_c$ was ~4–6 mm. $L_c$ decreased to zero as the 2D spiral wave approached its breakup regime.

Fig. 12 *C* shows the relationship between $\alpha_c$ and $L_z$ with $\bar{G}_{si}$ fixed at 0.045 mS/cm$^2$. $\alpha_c$ decreases as $L_z$ increases.

## Mechanisms of scroll breakup in 3D tissue

Using their simplified three-variable model, Fenton and Karma (1998a,b) showed that twiston-induced filament bending can lead to wavebreak and complex turbulent scroll behaviors in 3D tissue with rotational anisotropy due to fiber rotation. They expected that the mechanisms of filament bending and breaking "do not require specific forms of APD restitution curves." However, using the LR1 model, we find that a steep APD restitution curve is still one of the necessary conditions for the breakup, because neither a twisted scroll wave in a homogeneous tissue nor a scroll wave in tissue with fiber rotation broke up until the control parameter was increased to the 2D strong meander regime, in which APD restitution is steep. We develop our explanation for breakup in stages, as follows.

### *Tip meander in 2D*

As shown in Fig. 1, in 2D tissue, transitions from weak to strong meander to breakup occurred as the steepness of APD restitution increased. In the strong meander case, the spiral wave rotated with large oscillations in both wavelength and excitable gap due to steep APD restitution. This is illustrated in Fig. 13 *A* by snapshots of a spiral wave in the strong meander regime (corresponding to Fig. 1 *De*). Large differences in wavelength (*white-gray areas*) and excitable gap (*black areas*) along the spiral wave are evident, which did not occur in the stable or weak meander regimes (Fig. 13 *B*). In particular, the waveback in the weak meander regime was smooth, but "bumps" developed in the waveback during strong meander. These bumps were caused by the excitation of spatial modes due to the APD and conduction

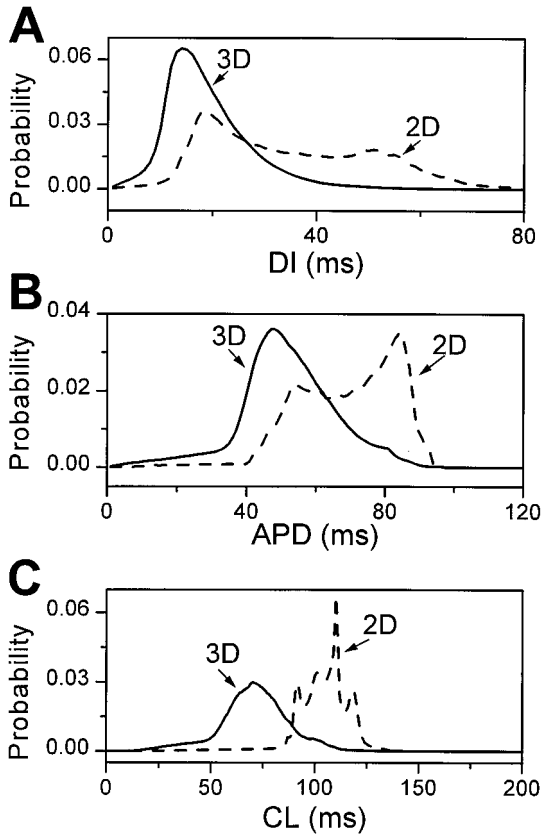


FIGURE 11 Probability distributions of average DI (*A*), APD (*B*), and CL (*C*) in the 2D strong meander regime. *Solid lines*: for the broken scroll waves in 3D tissue with fiber rotation shown in Figs. 9 and 10. *Broken lines*: for the 2D spiral wave shown in Fig. 1 *De* (*dashed lines*). The action potential parameters are identical in the two cases. DI, APD, and CL were recorded at every other grid point for a duration of 1 s in 3D and for 3 s in 2D.

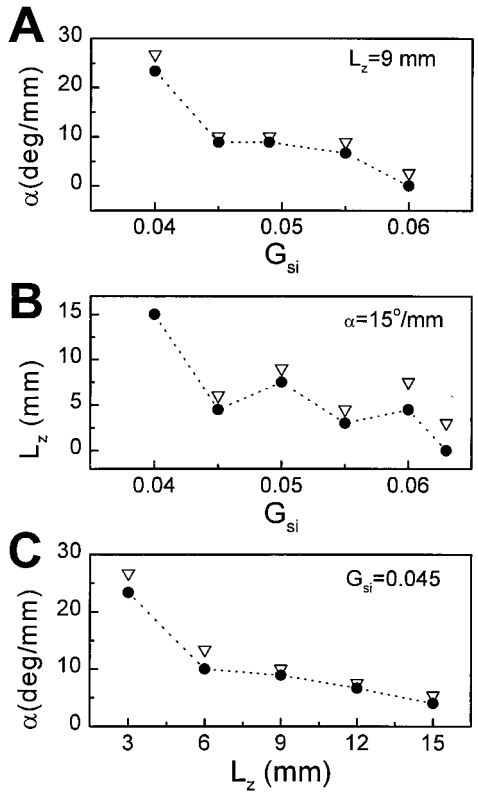


FIGURE 12 Relationships between 3D scroll behavior and $\bar{G}_{si}$ (controlling APD restitution steepness), fiber rotation rate $\alpha$, and tissue thickness $L_z$. ●, No breakup occurred; ▽, breakup occurred. We connected the full circles by dotted lines to distinguish the no-breakup and breakup regions; i.e., below the line is the no-breakup region, while above is the breakup region. (*A*) $\alpha$-$\bar{G}_{si}$ parameter space. (*B*) $L_z$-$\bar{G}_{si}$ parameter space. (*C*) $\alpha$-$L_z$ parameter space.

velocity restitution, as we have discussed previously (Qu et al., manuscript submitted for publication). Because of the meandering instability, the tip velocity of the spiral wave began to oscillate. Fig. 13 *C* compares spiral tip velocity for 2D spiral waves in the stable, weak meander, and strong meander regimes. When the spiral wave meandered, its tip velocity oscillated. In the strong meander regime, this oscillation became violent, varying from very fast (over 0.6 m/s) to extremely slow (close to zero). The slow phases corresponded to the spiral tip encountering a "bump" in the previous waveback (i.e., encountering relatively refractory tissue) (Fig. 13). With the tip in its slow phase, however, the core area had more time to recover, resulting in a larger excitable area (Figs. 13 *A*, *b*, *c*, and *f*). Therefore, once the tip had completed its slow turn, it moved into fully excitable tissue and propagated quickly and almost linearly (Figs. 13 *A*, *a*, *d*, and *g*). In contrast, in the weak meander regime, the tip was not slow enough in its slow phase to create such a large excitable gap in the core area as in the strong meander case.

### *How tip meander in 3D promotes filament bending*

Now let us explain how a scroll wave with a twisted filament breaks up in 3D homogeneous tissue. In homogeneous tissue, because we stacked spiral waves from different phases, the excitable areas and the tip velocities were different in each layer. The spiral waves in some layers were in the slow phase, and others were in the fast phase. When the scroll wave in a given layer completed its slow turn and began its fast movement, it faced excitable tissue not only in its own layer but also in the neighboring layers. If the gradient was large enough, then it invaded its neighboring layers and propagated in the $z$ direction, causing filament bending. This is illustrated in Fig. 14 *A*, where we show snapshots of different layers at $t = 28$ ms for the simulation in Fig. 5 *A*. At layers below $z = 2.4$ mm (Fig. 14 *Aa–c*), the spiral wave was still in its slow phase (trying to make the slow turn) and had a large excitable area in the center. However, the spiral waves in the layers above $z = 6$ mm had already completed the slow turn and moved into the fast phase (Fig. 14 *Af–h*). The spiral tips were thus able to propagate downward, causing a breakthrough-like excita-

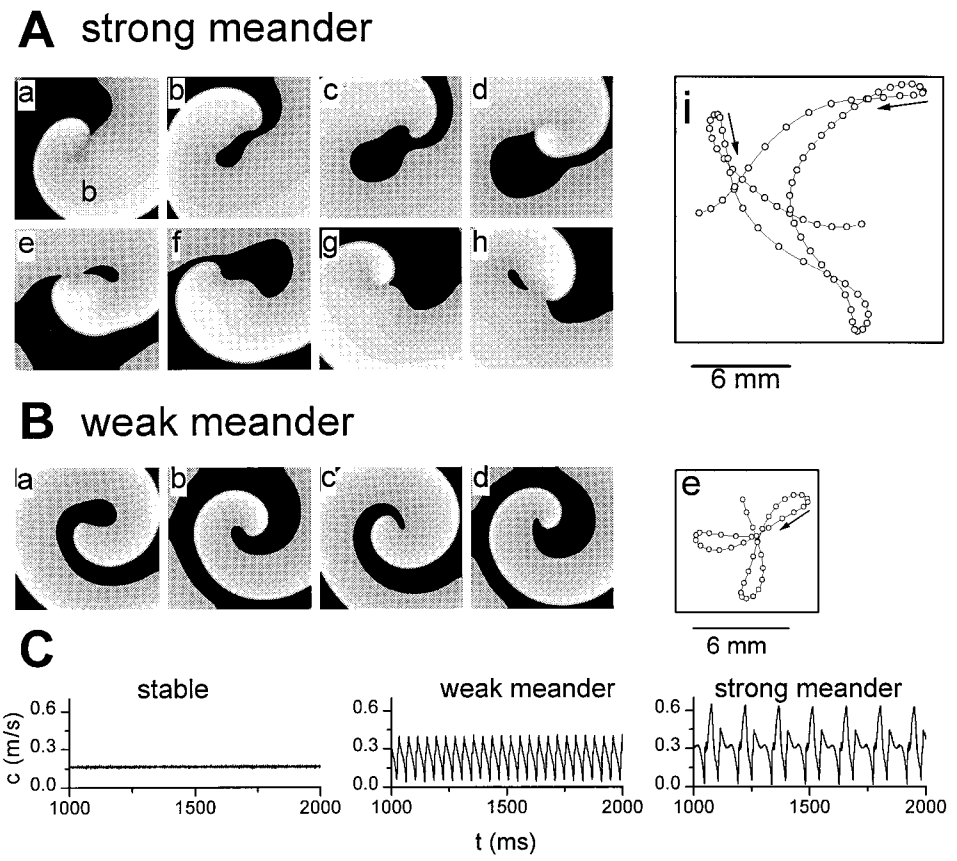


FIGURE 13 2D spiral tip movement. (*A*) Snapshots (every 20 ms) of a spiral wave in the strong meander regime (corresponding to Fig. 1 *De*). The panel at the far right shows the position of the spiral tip (*open circle*) every 3 ms, illustrating a slow phase (*closely spaced dots*) and a fast phase (*widely spaced dots*) of tip movement. Arrows indicate the turning from slow phase to fast phase. (*B*) Snapshots (every 30 ms) of a spiral wave in the weak meander regime (corresponding to Fig. 1 *Dc*). The panel at the far right shows much smaller differences between the fast and slow phases of tip movement than in *A*. (*C*) Tip velocity for a stable 2D spiral wave (for Fig. 1 *Da*), and for the weak and strong meander regimes in *A* and *B*. Tissue size: 4.8 cm $\times$ 4.8 cm. To show the excitable gap oscillation, we painted it black when $V < -70$ mV, which differs slightly from Fig. 1 *De*.

tion (Fig. 14 *Ac–e*). For such breakthrough excitation to occur, there must be large excitable gaps in the $z$ direction, due to different layers moving in different phases. This only occurs when the spiral wave is in the strong meander regime and when the spiral waves are sufficiently desynchronized by the twist of the filament. In the weak meander regime, the differences between the slow-moving and fast-moving phases of the tip are too small to generate large enough excitable gaps in the $z$ direction to cause filament bending sufficient to produce wavebreak.

In 3D tissue with fiber rotation, the mechanism of filament bending is similar. As was shown in Fig. 8, fiber rotation itself did not add new instability to the scroll wave dynamics unless it was extremely large. But for initial conditions of an untwisted scroll wave, fiber rotation caused the filament to twist (Fig. 9). The scroll wave thereby began to move in different phases in different layers, similar to the motion of an initially twisted scroll in homogeneous tissue. Fig. 14 *B* illustrates the filament bending process at $t = 42$ ms for the simulation shown in Fig. 9. The spiral waves in layers below $z = 3.6$ mm had completed their slow turn and moved to the fast phase, but the spiral waves in the layers above $z = 6$ mm were still in their slow turn, creating a very large excitable area in the core region. Therefore, a breakthrough could move upward, bending the filament. Fig. 14 *C* shows the local maxima and minima in the $z$ direction of the filaments for the simulation in Fig. 9 from $t = 20–60$ ms. At $t = 25$ ms, the filament began to bend. The minimum decreased a little at first and then remained nearly constant, while the maximum increased almost linearly. At $t = 54$ ms, the bending filament broke, forming a scroll ring and a scroll with a bent filament. At $t = 58$ ms, the filament unbended, and the scroll ring shrank and disappeared at $t = 60$ ms. That the minimum did not decrease indicated that there was no excitable gap for the filament to propagate downward. However, the filament propagated upward with an almost constant velocity ($\sim$0.15 m/s), indicating that there was excitable tissue available for propagation.

### *How filament bending promotes scroll breakup*

Once filament bending starts, there are several processes that can lead to scroll breakup. If the tissue is not thick, the bend in the filament can propagate to the boundary, where it may break in two (Fenton and Karma, 1998a,b). If the tissue is thick, however, a scroll ring may occur as a result of the bent filament colliding with itself (Figs. 5 *A* and 9). The scroll ring can either expand until it hits the boundaries to cause further filament break (Fig. 9) or shrink and disappear (Figs. 5 *A* and 9), depending on the twist rate. An important consequence of filament bending is the invasion of the excitable tissue from the $z$ direction, which makes the

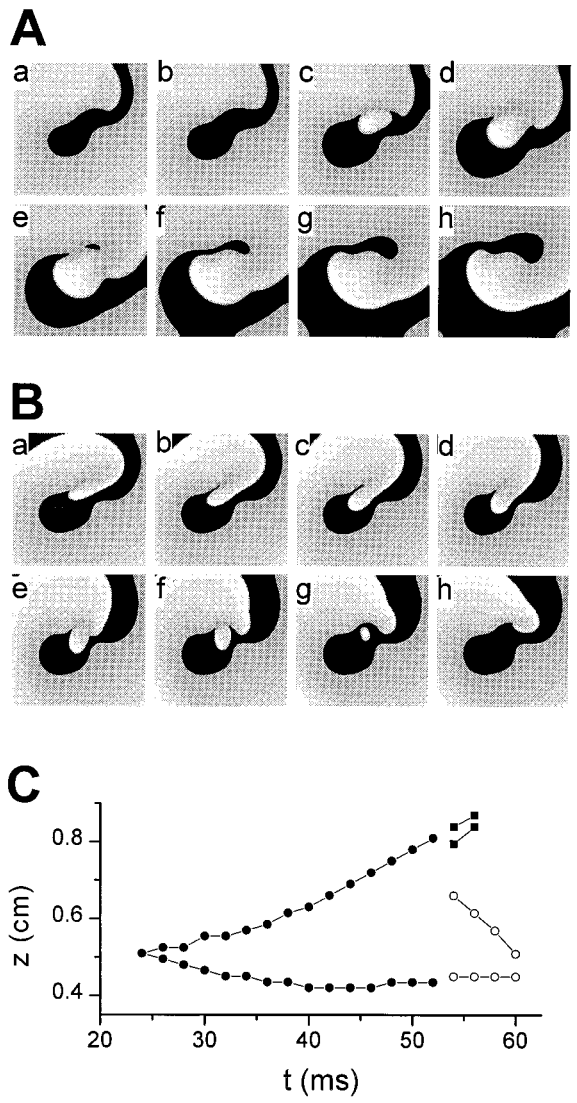


FIGURE 14 Simultaneous snapshots of a scroll wave at different depths, illustrating gradients in excitability along the $z$ axis caused by out-of-phase fast and slow tip movements, for the 2D strong meander regime. The same gray scale as in Fig. 13 was used. (*A*) $t = 28$ ms for homogeneous 3D tissue with the initial filament twisted (the simulation shown in Fig. 5). (*B*) $t = 42$ ms for 3D tissue with fiber rotation (the simulation shown in Fig. 9). *a–h* are layers equally distanced from lower "endocardial" to the top "epicardial" surface. (*C*) Local maxima and minima in the $z$ axis of the scroll filaments, from $t = 20$ to 60 ms, for *B*.

DI shorter than it would be without this invasion. This effectively shortens both APD and CL and thus moves the system into the steeper range of the APD restitution curve, promoting further restitution-induced instabilities. This shortening of CL due to $z$ direction reentry is a major cause of further wavebreak (Figs. 5 *B* and 9), following the first filament bending. These wavebreaks occur in the scroll arm, which is similar to the behavior of the wavebreaks in 2D spiral wave breakup. They are not due to a bent filament colliding with itself or with boundaries, but to conduction block in the spiral arm as a direct result of steep APD restitution. This kind of wave break in 3D can form either a scroll ring (e.g., $t = 400$ ms in Fig. 9) or a U-shaped scroll filament (e.g., $t = 800$ ms in Fig. 9).

In addition, in homogeneous tissue, twist itself speeds up the scroll wave (Biktashev et al., 1994), thus shortening CL and engaging a steeper portion of the APD restitution curve. If the system is very close to 2D breakup, scroll breakup may occur because of this speedup. This is the case shown in Fig. 7, where there was no filament bending, but a scroll ring formed because of wavebreak in the scroll arm.

In tissue with fiber rotation, the CL of a scroll wave did not change as in a twisted scroll wave in homogeneous tissue, but here another factor facilitated wavebreak, namely curvature of the wave induced by fiber rotation. To illustrate how curvature changes with fiber rotation in a scroll wave, we simulated unidirectional conduction on the surface of a cylinder. We set the diffusion coefficient on the cylinder as if it were sliced out of the tissue with 3D fiber rotation. (Details of the mathematics are in Eq. 8). Fig. 15 *A* shows the isopotential lines of the wavefront and waveback. The

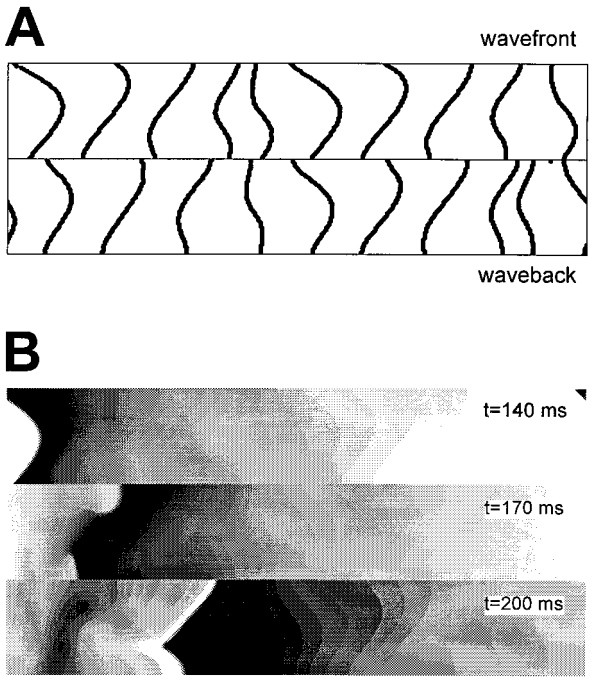


FIGURE 15 Wavefront and waveback dynamics during unidirectional reentry on the surface of a cylinder with fiber rotation, for the 2D strong meander regime. (*A*) Isochrones of the wavefront (*top*) and waveback positions (*bottom*) during successive cycles around the cylinder. Note that both wavefronts and wavebacks are curved. (*B*) Snapshots illustrating local wavebreak as a result of curvature mismatch (head-to-tail interaction) of the wavefront and waveback. At $t = 140$ ms, a convex wavefront approaches from the left; at $t = 170$ ms, wavebreak occurs when this wavefront encounters still-refractory tissue from the previous wave (due to curvature of its waveback); at $t = 200$ ms, the two broken wavefronts reseal.

curvatures of the wavefront and waveback changed constantly in both space and time. Curvature of a convex wave decreases conduction velocity but prolongs APD (Comtois and Vinet, 1999). Therefore, despite the same CL, APD prolongation in a curved wavefront makes conduction block easier. In addition, the waveback curvature may differ from the wavefront curvature at the same position. This allows conduction block to be localized to one region of the wavefront, resulting in a scroll ring in the tissue. Fig. 15 *B* shows such an episode of wavebreak in reentry on the cylinder. Because the conduction failure was very localized, the two spiral waves collided to heal the wavebreak. This corresponds to the case of the scroll ring shrinking in 3D tissue. If the break involves a sufficient large area, the two spiral waves continue to rotate, causing further wavebreaks to develop in the tissue.

## DISCUSSION

Scroll wave breakup has been proposed as a paradigm for the degeneration of tachycardia to fibrillation. In this study, we have investigated scroll wave stability by examining how 2D spiral waves behave when they are placed in 3D tissue under the following conditions: homogeneous 3D tissue in which the scroll wave has an initially straight filament; homogeneous 3D tissue in which the scroll wave has an initially twisted filament; and 3D tissue with fiber rotation (rotational anisotropy). Four phenotypes of 2D spiral waves were studied under these conditions: stable, weak meander, strong meander, and breakup. Because scroll wave behavior is model dependent (Qu et al., 1999b), we used a detailed cardiac action potential model incorporating physiologically based rather than phenomenologically based formulations of the key cardiac ionic currents.

From our findings, the major causes of the scroll breakup in this 3D model can be summarized as follows: 1) Steep APD restitution causes strong meander, thus promoting large oscillations in tip velocity that lead to large excitable gaps in the scroll core area. 2) Either fiber rotation or filament twist causes the scroll wave to move in different phases at different tissue depths, thereby creating gradients in excitability along the $z$ axis. 3) This allows transmural propagation in the $z$ direction, which causes the filament to bend. 4) If filament bending is large enough, the filament can break either by colliding with a border or by colliding intramurally with itself to produce a scroll ring. 5) Filament bending also fills in the large excitable gaps in the $z$ axis, thus effectively shortening the CL. If APD restitution slope is greater than 1 at these shorter CL's, then restitution-induced instabilities can cause wavebreak in the scroll arm, generating new scroll rings at a distance from the original filament. 6) In the stable or weak meander regime, scroll breakup does not occur because the excitable area of the core is not large enough to fit into two counterrotating spiral waves. 7) If the fiber rotation rate or initial filament twist is not large enough, then they do not create sufficient gradients to produce filament bending. For shallower APD restitution, a larger initial filament twist is required to induce scroll breakup. 8) Curvature of the scroll wavefront and waveback induced by fiber rotation also prolongs APD in localized regions, facilitating wavebreak along the scroll arm.

Based on the experimental results of Zipes et al. (1975) and Kavanagh et al. (1992), Winfree (1994a) has conjectured that tissue thickness is critical for scroll wave breakup. He suggested that a thickness threshold of one rotor diameter was necessary for instability to develop. We also find that 3D scroll breakup requires a critical tissue thickness, for the following reasons: 1) The maximum filament twist rates and gradients in excitability occur at 3–6 mm (Fig. 8, *C* and *D*, and Figure 9 in Fenton and Karma, 1998b). Therefore, a certain thickness is needed to develop sufficient twist for filament bending and scroll breakup. 2) In thin tissue, the degree to which the filament can bend is limited before it hits a surface boundary and disappears. However, we find that tissue thickness promotes scroll breakup only when the 2D spiral wave is in the strong meander regime. In the stable or weak meander regime, scroll waves do not break up at any tissue thickness, within the tissue size limits we have studied. In the strong meander regime, however, breakup occurs at thicknesses much smaller (typically 5 mm; see Fig. 12) than in the core meandering range (typically 10 mm; see Fig. 1 *D*).

Fenton and Karma (1998a,b) have shown that fiber rotation can be a major factor destabilizing scroll wave reentry, by causing filament bending leading to wavebreak. Although we also find that fiber rotation causes filament bending, we argue that fiber rotation does not induce new instabilities. Rather, its role is to induce and maintain filament twist and thus to convert instabilities arising from steep APD restitution into 3D scroll breakup. Supporting this argument is the observation that scroll breakup in tissue with fiber rotation is very similar to scroll breakup in homogeneous tissue with an initially twisted filament. In both cases, the effect is to shift the CL to shorter values, where APD restitution is steep enough ($>1$) to produce wavebreak. In homogeneous 3D tissue, straight filaments are stable, so that if twisted filaments finally become untwisted, breakup stops. This accounts for the transient nature of breakup in Fig. 6 (although we have not been able to substantiate that breakup is transient in all cases, because of computational time limitations.) In contrast to an initially twisted scroll in homogeneous tissue, in 3D tissue with fiber rotation, the fiber rotation continuously generates twist, so the breakup processes never stop. Therefore, the role of fiber rotation is to induce and maintain twist in 3D, thus facilitating the induction and maintenance of turbulent wave behavior. But only if APD restitution is sufficiently steep does fiber rotation or tissue thickness promote scroll breakup. In the stable or weak meander regimes, scroll waves always remained intact in this cardiac model.

We want to point out that in studying the effects of fiber rotation, we have used only one type of initial condition, i.e., a straight scroll wave perpendicular to fiber direction. Recent simulations by Berenfeld and Pertsov (1999) using the FHN model showed that a stable scroll filament tends to align with the fiber direction. Using the LR1 model, however, we never observed this to occur when the initial filament was set perpendicular to fiber direction (Fig. 8). In fact, no-flux boundary conditions on the lower "endocardial" and upper "epicardial" surfaces make the filament perpendicular to the fiber direction, as long as the two ends of the filament remain on the endocardial and epicardial surfaces. Only when the two ends of the filament are located on the sides of the tissue can alignment of the filament along fiber direction occur. It is noteworthy that in the real heart (in contrast to the cube simulated by Berenfeld and Pertsov (1999)), the epicardium and endocardium account for the great majority of the no-flux boundary surface area (even in isolated tissue preparations). Therefore the likelihood that a scroll filament will align parallel to the fiber direction is very small in the real heart, justifying our (and others') choice of initial conditions with the filament ends located on the endocardial and epicardial surfaces. In addition, we point out that in the present simulations, the occurrence of filament breakup due to collision with side walls is not likely to occur in the real heart, because the only boundaries that filaments can collide with in the real heart are the epicardium and endocardium.

Finally, some limitations should be mentioned. First, the LR1 model is not complete, lacking the full complement of time-dependent $K^+$ currents and detailed intracellular $Ca^{2+}$ dynamics, which may be very important for cardiac arrhythmias. Second, we treated cardiac tissue as a continuum and integrated the PDE, using a 0.15-mm spatial step. However, cardiac tissue is not a continuum, but is built up by discrete cells (approximate dimensions 0.15 mm $\times$ 0.02 mm $\times$ 0.01 mm) and includes bidomain features, which were not included here. Third, and most important, to analyze the essential features governing scroll wave dynamics, we did not include many important features of real cardiac tissue. These include the His-Purkinje system, transmural or base-to-apex electrophysiological differences (Antzelevitch et al., 1991; Laurita et al., 1996), realistic anatomical structure, etc. Furthermore, additional electrophysiological heterogeneities can be induced by drugs or disease, as well as anatomical heterogeneities. Further investigation will be required to assess the relevance of the present findings to scroll wave dynamics under realistic physiological and pathophysiological conditions. Although these other conditions have not yet been studied in detail, the findings of the present study are nevertheless encouraging. They lend hope to the concept that APD restitution steepness may be a global parameter regulating dynamical instability, which promotes scroll wave breakup. From a therapeutic standpoint, attempts to prevent wavebreak by altering APD restitution with drugs are much more practical than preventing wavebreak by eliminating tissue heterogeneities. Therefore, targeting the APD restitution could be a highly effective strategy for pharmacological therapy of cardiac fibrillation and sudden cardiac death, as suggested by recent experimental studies (Riccio et al., 1999; Garfinkel et al., *PNAS*, in press).

This research was supported by NIH SCOR in Sudden Cardiac Death P50 HL52319; by a Beginning Grant-in-Aid (to ZQ) and a Fellowship (to FX) from the American Heart Association, Western States Affiliate; and by the Laubisch and Kawata Endowments. Most of simulations were done on the massively parallel supercomputers jointly at the San Diego Supercomputing Center and the Maui High Performance Computing Center.

## REFERENCES

Allessie, M. A., F. I. M. Bonke, and F. J. C. Schopman. 1973. Circus movement in rabbit atrial muscle as a mechanism of tachycardia. *Circ. Res.* 33:54–77.

Antzelevitch, C., S. Sicouri, S. H. Litovsky, A. Lukas, S. C. Krishnan, J. M. Di Diego, G. A. Gintant, and D. W. Liu. 1991. Heterogeneity within the ventricular wall. Electrophysiology and pharmacology of epicardial, endocardial, and M cells. *Circ. Res.* 69:1427–1449.

Aranson, I. S., and A. R. Bishop. 1997. Instability and stretching of vortex lines in the three-dimensional complex Ginburg-Landau equation. *Phys. Rev. Lett.* 79:4174–4177.

Berenfeld, O., and A. M. Pertsov. 1999. Dynamics of intramural scroll waves in three-dimensional continuous myocardium with rotational anisotropy. *J. Theor. Biol.* 199:383–394.

Biktashev, V. N. 1998. A three-dimensional autowave turbulence. *Int. J. Bifurcation Chaos. Appl. Sci. Eng.* 8:677–684.

Biktashev, V. N., A. V. Holden, and H. Zhang. 1994. Tension of organizing filaments of scroll waves. *Philos. Trans. R. Soc. Lond. A.* 347: 611–630.

Chen, P. S., A. Garfinkel, J. N. Weiss, and H. S. Karagueuzian. 1997. Spirals, chaos, and new mechanisms of wave propagation. *PACE.* 20: 414–421.

Chen, P.-S., P. D. Wolf, E. G. Dixon, N. D. Danieley, D. W. Frazier, W. M. Smith, and R. E. Ideker. 1988. Mechanism of ventricular vulnerability to single premature stimuli in open chest dogs. *Circ. Res.* 62:1191–1209.

Chudin, E., J. Goldhaber, A. Garfinkel, J. Weiss, and B. Kogan. 1999. Intracellular $Ca^{2+}$ dynamics and the stability of ventricular tachycardia. *Biophys. J.* 77:2930–2941.

Comtois, P., and A. Vinet. 1999. Curvature effects on activation speed and repolarization in an ionic model of cardiac myocytes. *Phys. Rev. E.* 60:4619–4628.

Courtemanche, M. 1996. Complex spiral wave dynamics in a spatially distributed ionic model of cardiac electrical activity. *Chaos.* 6:579–600.

Courtemanche, M., L. Glass, and J. P. Keener. 1993. Instabilities of a propagating pulse in a ring of excitable media. *Phys. Rev. Lett.* 70: 2182–2185.

Davidenko, J. M., A. M. Pertsov, R. Salomonsz, W. Baxter, and J. Jalife. 1992. Stationary and drifting spiral waves of excitation in isolated cardiac muscle. *Nature.* 355:349–351.

Ding, M., and W. Yang. 1997. Stability of synchronous chaos and on-off intermittency in coupled map lattices. *Phys. Rev. E.* 56:4009–4016.

Efimov, I. R., V. I. Krinsky, and J. Jalife. 1995. Dynamics of rotating vortices in the Beeler-Reuter model of cardiac tissue. *Chaos Solitons Fractals.* 5:513–526.

Fenton, F., and A. Karma. 1998a. Fiber-rotation-induced vortex turbulence in thick myocardium. *Phys. Rev. Lett.* 81:481–484.

Fenton, F., and A. Karma. 1998b. Vortex dynamics in three-dimensional continuous myocardium with fiber rotation: filament instability and fibrillation. *Chaos.* 8:20–47.

Garfinkel, A., P. S. Chen, D. O. Walter, H. S. Karagueuzian, B. Kogan, S. J. Evans, M. Karpoukhin, C. Hwang, T. Uchida, M. Gotoh, O. Nwasokwa, P. Sager, and J. N. Weiss. 1997. Quasiperiodicity and chaos in cardiac fibrillation. *J. Clin. Invest.* 99:305–314.

Garfinkel, A., and Z. Qu. 1999. Nonlinear dynamics of excitation and propagation in cardiac muscle. *In* Cardiac Electriophysiology: From Cell to Bedside. D. P. Zipes and J. Jalife, editors. W. B. Saunders Co., Philadelphia. 315–320.

Gray, R. A., and J. Jalife. 1998. Ventricular fibrillation and atrial fibrillation are two different beasts. *Chaos.* 8:65–78.

Gray, R. A., J. Jalife, A. V. Panfilov, W. T. Baxter, C. Cabo, J. M. Davidenko, A. M. Pertsov, and A. T. Winfree. 1995. Mechanisms of cardiac fibrillation. *Science.* 270:1222–1225.

Gray, R. A., A. M. Pertsov, and J. Jalife. 1998. Spatial and temporal organization during cardiac fibrillation. *Nature (Lond.).* 392:75–78.

Heagy, J. F., L. M. Pecora, and T. L. Carroll. 1995. Short wavelength bifurcations and size instabilities in coupled oscillator systems. *Phys. Rev. Lett.* 74:4185–4188.

Hu, G., Z. Qu, and K. He. 1995. Feedback control of chaos in spatiotemporal systems. *Int. J. Bifurcation Chaos. Appl. Sci. Eng.* 5:901–936.

Jafri, M. S., J. J. Rice, and R. L. Winslow. 1998. Cardiac $Ca^{2+}$ dynamics: the roles of ryanodine receptor adaptation and sarcoplasmic reticulum load. *Biophys. J.* 74:1149–1168.

Janse, M. J., and A. L. Wit. 1989. Electrophysiological mechanisms of ventricular arrhythmias resulting from myocardial ischemia and infarction. *Physiol. Rev.* 69:1046–1169.

Karma, A. 1994. Electrical alternans and spiral wave breakup in cardiac tissue. *Chaos.* 4:461–472.

Kavanagh, K. M., J. S. Kabas, D. L. Rollins, S. B. Melnick, W. M. Smith, and R. E. Ideker. 1992. High-current stimuli to the spared epicardium of a large infarct induce ventricular tachycardia. *Circulation.* 85:680–698.

Keener, J. P., and J. Tyson. 1992. The dynamics of scroll waves in excitable media. *SIAM Rev.* 34:1–39.

Kim, Y. H., A. Garfinkel, T. Ikeda, T. J. Wu, C. A. Athill, J. N. Weiss, H. S. Karagueuzian, and P. S. Chen. 1997. Spatiotemporal complexity of ventricular fibrillation revealed by tissue mass reduction in isolated swine right ventricle. Further evidence for the quasiperiodic route to chaos hypothesis. *J. Clin. Invest.* 100:2486–2500.

Laurita, K. R., S. D. Girouard, and D. S. Rosenbaum. 1996. Modulation of ventricular repolarization by a premature stimulus. Role of epicardial dispersion of repolarization kinetics demonstrated by optical mapping of the intact guinea pig heart. *Circ. Res.* 79:493–503.

Lee, J. J., K. Kamjoo, D. Hough, C. Hwang, W. Fan, M. C. Fishbein, C. Bonometti, T. Ikeda, H. S. Karagueuzian, and P. S. Chen. 1996. Reentrant wave fronts in Wiggers' stage II ventricular fibrillation. Characteristics and mechanisms of termination and spontaneous regeneration. *Circ. Res.* 78:660–675.

Luo, C. H., and Y. Rudy. 1991. A model of the ventricular cardiac action potential: depolarization, repolarization, and their interaction. *Circ. Res.* 68:1501–1526.

Luo, C. H., and Y. Rudy. 1994. A dynamical model of the cardiac ventricular action potential. I. simulations of ionic currents and concentration changes. *Circ. Res.* 74:1071–1096.

Muzikant, A. L., and C. S. Henriquez. 1998. Bipolar stimulation of a three-dimensional bidomain incorporating rotational anisotropy. *IEEE Trans. Biomed. Eng.* 45:449–462.

Nam, K., E. Ott, P. N. Guzdar, and M. Gabbay. 1998. Stability of spiral wave vortex filaments with phase twists. *Phys. Rev. E.* 58:2580–2585.

Panfilov, A. V., and A. V. Holden. 1997. Computational Biology of the Heart. Wiley, New York.

Panfilov, A. V., and J. P. Keener. 1995. Reentry in three-dimensional Fitzhugh-Nagumo medium with rotational anisotropy. *Physica D.* 84: 545–552.

Pollard, A. E., M. J. Burgess, and K. W. Spitzer. 1993. Computer simulations of three-dimensional propagation in ventricular myocardium: effects of intramural fiber rotation and inhomogeneous conductivity on epicardial activation. *Circ. Res.* 72:744–756.

Qu, Z., and A. Garfinkel. 1999. An advanced numerical algorithm for solving partial differential equation in cardiac conduction. *IEEE Trans. Biomed. Eng.* 49:1166–1168.

Qu, Z., J. N. Weiss, and A. Garfinkel. 1999a. Cardiac electrical restitution properties and the stability of reentrant spiral waves: a simulation study. *Am. J. Physiol.* 276:H269–H283.

Qu, Z., F. Xie, and A. Garfinkel. 1999b. Diffusion-induced 3-dimensional vortex filament instability in excitable media. *Phys. Rev. Lett.* 83: 2668–2671.

Quan, W., S. J. Evans, and H. M. Hastings. 1998. Efficient integration of a realistic two-dimensional cardiac tissue model by domain decomposition. *IEEE Trans. Biomed. Eng.* 45:372–385.

Riccio, M. L., M. L. Koller, and R. F. Gilmour, Jr. 1999. Electrical restitution and spatiotemporal organization during ventricular fibrillation. *Circ. Res.* 84:955–963.

Rush, S., and H. Larsen. 1978. A practical algorithm for solving dynamic membrane equations. *IEEE Trans. Biomed. Eng.* 25:389–392.

Vetter, F. J., and A. D. McCulloch. 1998. Three-dimensional analysis of regional cardiac function: a model of rabbit ventricular anatomy. *Prog. Biophys. Mol. Biol.* 69:157–183.

Vigmond, E. J., and L. J. Leon. 1999. Computationally efficient model for simulating electrical activity in cardiac tissue with fiber rotation. *Ann. Biomed. Eng.* 27:160–170.

Weiss, J. N., A. Garfinkel, H. S. Karagueuzian, Z. Qu, and P. S. Chen. 1999. Chaos and the transition to ventricular fibrillation: a new approach to antiarrhythmic drug evaluation. *Circulation.* 99:2819–2826.

Winfree, A. T. 1994a. Electrical turbulence in three-dimensional heart muscle. *Science.* 266:1003–1006.

Winfree, A. T. 1994b. Persistent tangled vortex rings in generic excitable media. *Nature.* 371:233–236.

Witkowski, F. X., L. J. Leon, P. A. Penkoske, W. R. Giles, M. L. Spano, W. L. Ditto, and A. T. Winfree. 1998. Spatiotemporal evolution of ventricular fibrillation. *Nature.* 392:78–82.

Xu, A., and M. R. Guevara. 1998. Two forms of spiral wave reentry in an ionic model of ischemic ventricular myocardium. *Chaos.* 8:157–174.

Yang, J., G. Hu, and J. Xiao. 1998. Chaos synchronization in coupled chaotic oscillators with multiple positive Lyapunov exponents. *Phys. Rev. Lett.* 80:496–499.

Zipes, D. P., J. Fischer, R. M. King, A. Nicoll, and W. W. Jolly. 1975. Termination of ventricular fibrillation in dogs by depolarizing a critical amount of myocardium. *Am. J. Cardiol.* 36:37–44.